Hydrol. Earth Syst. Sci. Discuss., 8, 5123–5163, 2011
www.hydrol-earth-syst-sci-discuss.net/8/5123/2011/
doi:10.5194/hessd-8-5123-2011

Hydrology and Earth System Sciences Discussions

A combined field and modeling study of groundwater flow in a tidal marsh

Yuqiang Xia[1,2] **and Hailong Li**[3,2]

[1]State Key Laboratory of Biogeology and Environmental Geology, China University of Geosciences, Wuhan 430074, China
[2]Center for Natural Resources Development and Protection (NRDP), Department of Civil and Environmental Engineering, Temple University, PA 19122, USA
[3]State Key Laboratory of Biogeology and Environmental Geology, China University of Geosciences-Beijing, Beijing 100083, China

Received: 11 May 2011 – Accepted: 20 May 2011 – Published: 24 May 2011

Correspondence to: Hailong Li (hailongli@cugb.edu.cn)

Published by Copernicus Publications on behalf of the European Geosciences Union.

Abstract

Bald mud beaches were found among the mangrove marshes in Dongzhaigang National Nature Reserve, Hainan, China. To investigate the possible reasons for this phenomenon, the intertidal zones of a mangrove transect and a bald beach transect with similar topography and same tidal actions were selected for comparison study. Along both transects, observed water table variations were significant in the high and low intertidal zones and negligible in the middle intertidal zones. Field investigations and observations invite two speculations: (1) existence of a high-permeability zone on each transect which underlies the low-permeability surface mud sediments and outcrops in the high intertidal zone, and (2) considerable inland freshwater recharge along the mangrove transect but negligible freshwater recharge along the bald beach transect. Two-dimensional numerical simulations based on these speculations gave results in line with the observed water table. The bald beach is most probably due to the lack of enough freshwater for generating a brackish beach soil condition essential to mangrove growth. It is also indicated that seawater infiltrated the high-permeability zone through its outcrop near the high intertidal zone, and discharged from the tidal river bank in the vicinity of the low tide line, thereby forming a tide-induced seawater-groundwater circulation which may provide considerable contribution to the total submarine groundwater discharge.

1 Introduction

Salt marshes perform a variety of functions such as maintaining biodiversity, stabilizing and recycling nutrients and organic carbon, buffering storms and hurricanes, and providing nursery areas for marine fauna and flora (Valiela and Teal, 1979; Steudler and Peterson, 1984; Luther et al., 1986; Dittmar et al., 2006; Kristensen et al., 2008; Nagelkerken et al., 2008). They have attracted numerous scientific investigations, particularly in salt marsh ecology (Chapman, 1938, 1940; Lugo and Snedaker, 1974),

HESSD
8, 5123–5163, 2011

which includes many interesting and important issues such as salt marsh dieback and plant zonation (Mendelssohn et al., 1981; Dacey and Howes, 1984; Pennings and Callaway, 1992; Costa et al., 2003; Silvestri et al., 2005; Alber et al., 2008). As one of the most important salt marsh ecosystems, mangrove marshes typically occur along tidal estuaries and coastlines in tropical and subtropical regions (Chapman, 1977; Woodroffe et al., 1985; Kjerfve, 1990; Spalding et al., 1997). They are important for coastal ecology and play an important and irreplaceable role in the maintenance of coastal biodiversity (Field et al., 1998; Bosire et al., 2008). However, mangrove forests are also one of the world's most threatened tropical ecosystems with an obvious global degradation (Valiela et al., 2001; Liu and Diamond, 2005; Duke et al., 2007; Gilman et al., 2008) due to increasing anthropogenic activities such as global warming and sea level rising (Kjerfve, 1990; Duke et al., 1998; Krauss et al., 2008).

Both surface and ground freshwater are important for controlling the salinity and nutrient transport in mangrove tidal marshes around the world. Due to the observed enhanced size of mangrove trees along rivers, mangroves are believed to obtain their nutrients from freshwater runoff (Wolanski and Ridd, 1986). Kjerfve (1990) reported that the input of freshwater is ultimately responsible for creation of the brackish to saline coastal wetland environment where mangrove thrives. Previous researches have demonstrated that tide with brackish water combined with river runoff of freshwater has a significant effect in the form/exchanges of nutrient and material between mangrove and other ecosystems. Nuttle and Harvey (1995) reported the upward discharge of fresh groundwater on the water and solute movements within an intertidal wetland in Virginia Coast Reserve Long Term Ecological Research site on Virginia's Atlantic coast. They found that groundwater-driven advection will prevent infiltration of brackish water during tidal flooding and remove salt and other solutes from the sediment of wetland. Kitheka (1996) concluded that the river input of freshwater which is normally associated with high nutrient partly sustains the coastal biotopes (mainly mangroves and seagrass) in the mangrove-dominated Gazi Bay, southern Kenya. Hoguane et al. (1999) reported detailed measurements of the hydrodynamic regime, temperature

HESSD
8, 5123–5163, 2011

and salinity in the Ponta Rasa Mangrove Swamp, Mozambique, and confirmed that the hydrodynamics of the mangrove marsh are controlled by the tides, friction by the mangrove trees and the geometry of the connecting tidal creek. Selvam (2003) examined the variations in the periodicity and quantity of freshwater flowing into mangrove wetlands in India, and found that the reduction in freshwater flow would lead to reduction in the diversity of exclusive mangrove plant species. Montalto et al. (2006) presented the hydrological characteristics of the Piermont Marsh in the Hudson River Estuary, New York, USA. Schwendenmann et al. (2006) found that the sediment permeability and freshwater input had a strong effect on the solute dynamics (e.g., salt content) in tidal creek and mangrove water and on the vertical distribution in the sediment in a mangrove in North Brazil (Furo do Meio, Para). Acting as a main carrier of salt and nutrients, groundwater flow plays a significant role in the mass fluxes across the sediment-water interface and therefore affects the tidal marsh ecological system (Hemond and Fifield, 1982; Howes et al., 1996; Gardner, 2005; Wilson and Gardner, 2006; Akamatsu et al., 2009).

In many tidal marsh systems in the world, high-permeability zones were found under the surface marsh mud and they usually consist of sands or sandy loam (e.g., Harvey et al., 1987; Hughes et al., 1998; Gardner and Porter, 2001; Xin et al., 2009). Gardner and Porter (2001) reported that marsh mud commonly overlies a sand layer in the southeastern United States. Schwendenmann et al. (2006) also found that the permeability of deeper fine sand strata in a mangrove in North Brazil was 7 to 18 times larger than that of the upper mud layer ($<0.1\,\mathrm{m\,day^{-1}}$). Gardner (2007) noted that the presence of the sand layer beneath marsh mud is likely to increase seepage from marsh soils and enhances lowering of the water table and thereby increases aeration throughout the marsh. This kind of high-permeability zones might also contribute to the creation of a preferentially aerated layer under the plant roots (Tossatto et al., 2009).

In Dongzhaigang National Nature Reserve, Hainan Island, China, most mangroves distribute on the broad shallow beach such as Sanjiang plain and the coastal area of Tashi (Fig. 1a), other mangrove forests are situated along the river (e.g., Yanfeng River,

HESSD
8, 5123–5163, 2011

Fig. 1b). However, bald beaches without any vegetation were found among these mangrove marshes. In order to investigate the hydrogeological factors leading to the bald beaches, a mangrove transect and bald beach transect were selected to conduct field study for comparison (Fig. 1b). The mangrove transect is located in Changningtou tidal marsh, and adjacent to the estuary of Yanfeng River. The bald beach transect is situated in a tidal beach without any vegetation and abuts the Shanweitou Village and Dongzhaigang Bay. Along each transect, 8 ~ 9 observation wells were installed and then the water level in the wells was measured for three days with intervals of 1 ~ 3 h. The finite element model MARUN (MARine UNsaturated, Boufadel et al., 1999) was used to simulate the observed water tables. By mean of comparisons of the water table along the two transects, we discussed the ecohydrological implications related to the observations such as seawater-groundwater interaction, beach permeability distribution, marsh soil aeration conditions, marsh plant zonation, freshwater recharge from inland, and submarine groundwater discharge (SGD). Based on the discussions, the main factors leading to the bald beach were identified.

2 Study sites

Dongzhaigang National Nature Reserve, a subtropical tidal wetland with curved coastlines and gentle harbors, is the first mangrove forest reserve in China founded in 1980 and located in north-eastern Hainan Island, about 32 km from Haikou City. Its geographical coordinates are 19°57′–20°01′ N, 110°32′–110°37′ E (Fig. 1a). Tides in this area are mixture of diurnal and semidiurnal components. The tidal range is about 1.92 m during spring tides and 0.38 m during neap tides (NMDIS, 2008). Dongzhaigang is a shoalwater bay formed by continental sink during the 1605 Great Qiongzhou Earthquake, and has a typical subtropical monsoon marine climate. With 2065 km^2 of mangrove forests distributed in the shoals of the tidal zone, Dongzhaigang National Nature Reserve accounts for 44.51 % of mangrove forests of Hainan Island and is the largest and best mangrove forest nature reserve in China. Its annual average rainfall is

HESSD
8, 5123–5163, 2011

1700–1933 mm (data during 1973–1986) with 80 % of the precipitation occurring during May–October. The annual average temperature of the surface sea water is around 24.5°C (Fu, 1995). The mangrove marshes in Dongzhaigang National Nature Reserve mainly distribute in three coastal areas: Tashi, Yanfeng and Sanjiang Plain (Fig. 1a).

Two transects were selected for field investigations in Yanfeng and their distance is about 1.8 km (Fig. 1b). The first (mangrove transect) is located in Changningtou mangrove tidal marsh, and adjacent to the estuary of Yanfeng River. Mangrove plant species in this site mainly include *Aegiceras corniculatum*, *Bruguiera sexangula*, *Bruguiera gymnorrhiza*, *Kadelia candel*, *Ceriops tagal* and *Acanthus ilicifolius* (Ye and Lu, 2001). Nine monitoring wells (M0-M8) were installed along the mangrove transect (M-M′ in Figs. 1b, 2a) perpendicular to the high tide mark. Well M0 is located at the intersection of mangrove marsh and inland hill. The width of intertidal zone is about 100.0 m (Fig. 2a). The second (bald beach transect) is situated in a tidal beach without any vegetation. It abuts the Shanweitou Village and Dongzhaigang Bay. The beach sediment is mainly mud. Eight monitoring wells (B0-B7) were set up in the bald beach transect perpendicular to the high tide mark (B-B′ in Figs. 1b, 2b). The width of intertidal zone is about 190.0 m (Fig. 2b).

3 Methods

Boreholes were drilled with Hand Auger (AMS Inc., USA) to install observation wells. The depths of the boreholes are 2.0 m in intertidal zones of both transects and 4.0 m landward of the high tide mark of the bald beach transect. Landward of the high tide mark of the mangrove transect, only very shallow boreholes could be drilled with Hand Auger due to hard rocks encountered below the thin (0.5 ∼ 0.8 m) soil cover. A 1.0 m wide and 1.0 m long pit was excavated there and volcanic basalt boulders were found below the thin soil cover, which prevented us from further excavating to find the inland water table.

HESSD
8, 5123–5163, 2011

Each well was made up of inner and outer PVC pipes (Fig. 3). The diameter of the outer pipe is 5 cm and that of the inner pipe is 3.8 cm. Holes with diameter of 5.0 mm were drilled evenly around the perimeters of the inner and outer PVC pipes with a density of 4 ~ 5 holes per 5 cm of the pipe's longitudinal length. Then outer and inner pipes were wrapped by fine plastic screen, and the inner pipe was put inside the outer one (Fig. 3). The space between the two pipes was filled with coarse sands (0.5 mm ~2 mm in diameter). When installing the well, the space between the borehole and the outer pipe was also filled with the same coarse sands. All these measures were taken in order to prevent the fine beach sediments from entering wells and to guarantee good hydraulic connection between the beach pore water and the water inside the well. All the monitoring wells were installed during 12–17 December 2007, which provided 7 ~ 13 days for the disturbed groundwater level to recover to natural status. The elevations of wells and the topography of study profiles were geometrically leveled using Electronic Total Station (TOPCON, Japan) which has a measurement accuracy of ±2 mm. The data were summarized in Tables 1 and 2.

Water level in each well was measured for a 3-day period from 25 December 2007, 08:00 to 28 December 2007, 08:00. The distance between the top of well and the water table inside the well was measured with a plastic rod at the end of which an open circuit contact was installed. The open circuit would be closed when the contact at the end touched the water surface causing the oscillating of the pointer of a multimeter connected in the circuit. The error of water table measurements is less than 4 mm. The water level was measured with an interval of 1 h whenever the seawater depth at the well location was shallow enough to be accessed.

4 Field results

Our field observations were conducted during spring tides. There was no rainfall during the 3-day observation period. The tidal level (H_{Tide}) is represented by the following analytical expression:

HESSD
8, 5123–5163, 2011

$$H_{\text{Tide}}(t) = h_{\text{MSL}} + \sum_{i=1}^{5} A_i \cos(\omega_i t + \varphi_i), \quad (1)$$

where h_{MSL} denotes the mean sea level, A_i, ω_i and φ_i ($i = 1, \cdots, 5$) are the amplitude (m), frequency (rad/hour) and phase shift (rad) of the i-th component of tides, respectively, and their values were listed in Table 3. They were obtained using the least-squares fitting to the water table observed at the seaward wells in the beach (well M8 for the mangrove transect and B7 for the bald beach) when the surface of these well were submerged. After the tidal levels were determined, the lowest tidal level in each transect is defined as the elevation datum there ($z = 0$, Fig. 2). Here we used five harmonic tidal components (O1, K1, M2, S2, and N2, see Table 3) because they are important geophysically, together accounting for approximately 95 % of the total tidal potential (Merritt, 2004).

The observed time series of water levels along the two transects were reported in Figs. 4 and 5 together with the ground surface elevation and the analytical fitting of the tidal level. During high tides, the seawater was too deep at some wells in the middle and lower intertidal zone (such as M5-M8, and B3-B7) for these wells to be accessed, thus the measurements happened during only low tides. Water table variation patterns along the mangrove transect can be classified into two groups (Fig. 4): (1) quick dropping of water table during low tides and abrupt rising when the ground surface at the well was submerged by rising tides (M0 and M7); (2) very slow or negligible dropping of water table during low tides (M1-M6, and M8). Water table variation patterns along the bald beach can be classified into four groups (Figs. 4 and 5). (1) B0: slight daily fluctuation (amplitude smaller than 0.1 m, Fig. 5) around a very low elevation slightly higher than the lowest tidal level ($z = 0$ m); (2) B1-B3: quick dropping of water table during low tides and abrupt rising when the ground surface at the well was submerged by rising tides; (3) B6: mild dropping of water table during low tides and quick rising when the ground surface at the well was submerged by rising tides; and (4) the remainders (B4, B5, and B7): very slow or negligible dropping of water table during low tides.

HESSD
8, 5123–5163, 2011

Soil samples with 8 cm length and 7 cm diameter were collected at an interval of 5 cm during well installation and numbered sequentially. Table 4 summarizes the characteristics of soil samples collected from the bald beach transect. The sediments around B0 and the upper part of B1 are mainly compacted clay. Sediments at B2-B3 and the lower part of B1 are dominated by sandy loam with gravel. Mud sediments are extensively distributed on tidal platform (B4-B7). The sediments around M0 are dominated by sandy loam with gravel. The sediments in the intertidal zone of the mangrove transect (M1-M8) are almost uniform (mainly mud). The soil properties along the mangrove transect is much simpler than those along the bald beach transect and therefore are not tabulated.

5 Data analysis

5.1 Mangrove transect

The quick dropping of water table at M0 during low tides indicated the presence of a high-permeability zone there. The lowest water table at M0 was even lower than that at M1. Logically this may be caused by either landward drainage or possible presence of a high-permeability zone underlain the less-permeable marsh soil and the quick seaward drainage of the pore water around M0 through this zone (see the schematic illustration in Fig. 2a). In the field investigation, boulders (0.2–1.5 m in diameter) were exposed near the surface of M0 (Fig. 6). In addition, both hand auger drilling and big pit excavation landward of the M0 indicated that the inland area of the mangrove transect is underlain by a permeable aquifer consisting of boulders, which may extend the high-permeability zone landward and provide considerable freshwater recharge from inland.

The very slow or even negligible dropping of water table at M1-M6 during low tides was most probably due to the low-permeability of the marsh soil and the relatively flat soil surface of the mangrove marsh. Although there may exist a high-permeability zone below the marsh soil layer, it is possible that the low-permeability marsh soil and the

HESSD
8, 5123–5163, 2011

long, flat marsh platform between M1 and M6 lead to the negligible water table dropping during low tides.

The water table at M7 dropped quickly during low tides because (1) M7 is very near to the relatively steep bank and (2) the soil permeability near the tidal river bank (at least including the bottom of well M7) may be much higher than the inner marsh soil as illustrated in Fig. 2a (the loose bank zone (2)). The negligible dropping of water table at M8 during low tides was most probably due to the seepage face occurred there since the creek bed may be covered by the low-permeability mud sediments and the exit of seaward groundwater drainage from inland through the high-permeability zone underlain the marsh soil may be located near M8.

Many researchers have demonstrated that fresh groundwater discharge "tube" usually forms close to the low tide mark of an intertidal zone, and separate the saltwater wedge and the landward saline plume "hanging" beneath the beach surface of the intertidal zone (Boufadel, 2000; Robinson et al., 2006; Li et al., 2008). The high-permeability of the loose bank zone (zone (2) in Fig. 2a) is beneficial to the forming of the groundwater discharge tube.

5.2 Bald beach transect

The water table fluctuation at B0 was completely different from that at B1 (Fig. 5), although their spatial distance is very close (Fig. 2b). The water table at B0 fluctuated slightly with a range smaller than 0.2 m around the elevation of 0.25 m. The water table at B1 fluctuated with a much greater range of about 1.4 m ~ 1.5 m and was always greater or equal to that at B0, indicating that the groundwater flow direction between B0 and B1 was landward. The water table difference between B0 and B1 can be as large as ~1.4 m during high tides, indicating that the well B1 is located in a high-permeability zone with good hydraulic connection with the tidal water but well B0 is in a much less permeable zone with poor hydraulic connection with the tidal water. This speculation is also supported by the soil properties around these two wells (Table 4). Both aquifer slug tests and analytical study conducted by Guo et al. (2010) indicated that

HESSD
8, 5123–5163, 2011

the permeability (3.8×10^{-6} m s^{-1}) near B0 is about two orders of magnitude smaller than that (6.77×10^{-5} m s^{-1}) near B1. These observations and analyses indicate that the freshwater recharge from inland is negligible along this transect. The anomaly that the observed water table elevation at B0 was much lower than the mean sea level is probably due to unknown pumping of groundwater in inland area near the bald beach transect.

The observed water tables at wells B1-B3 dropped very quickly during falling tides and low tides and rose abruptly when the ground surface at the well was submerged by rising tides. The lowest water tables at B1-B3 were even much lower than that at B4, where the water table stayed near the ground surface during low tides. Due to the very poor hydraulic connection between B0 and B1, the only reasonable explanation for the quick dropping of water table at B1-B3 during low tides could be the presence of a high-permeability zone below the mud sediment of the bald beach, a scenario similar to the mangrove transect (see Figs. 2a and b). The pore water near B1-B3 drained quickly seaward through this high-permeability zone since the high-permeability zone outcrops in the higher intertidal zone including B1-B3. This is reasonable considering that the higher intertidal zone has much less tidal submersion periods than the middle or lower intertidal zone, causing much less silt and mud deposition the higher intertidal zone. Note that the water table at B1 was much lower than the tidal level during high tides, indicating a low-permeability zone covering the top part of B1. This was supported by the soil properties of sediments around B1 (Table 4).

The very slow or even negligible dropping of water table at B4 and B5 during low tides was most probably due to the low-permeability of the mud sediments and the relatively flat beach surface of the bald beach (see Fig. 2b). Although there may exist a high-permeability zone below the mud layer, it is possible that the low-permeability mud and the long, flat platform near B4 and B5 lead to the negligible water table dropping during low tides. The water table in B6 dropped considerably lower than beach surface during low tides and rose abruptly when the beach surface was submerged by rising tide. This was most probably due to the increase of the beach slope seaward of B6

HESSD
8, 5123–5163, 2011

(Fig. 2b). At B7, the water table remained as high as the ground surface during low tides. Note that the surface elevation of B7 is close to that of M8. Therefore, similar reason might lead to this negligible water table dropping: namely, seepage face might occur there due to seaward groundwater drainage of the seawater entering the outcrop of the high-permeability zone near B1, B2, and B3, and the loose bank zone similar to the mangrove transect (zone (2) in Fig. 2).

6 Numerical verification

In previous section, we obtained the following speculations based on the field investigations and observed water table: (1) Both the mangrove and bald beach transects have a similar macroscopical structure of two zones: a surface zone of low-permeability mud and an underlying high-permeability zone that outcrops at the high and low tide lines. (2) The fresh water recharge from inland is considerable along the mangrove transect but negligible along the bald beach transect. In order to verify these speculations, two-dimensional numerical simulations were conducted to match the observed water tables along both transects.

6.1 Implementation of numerical simulations

Numerical simulations were conducted using the MARUN model (Boufadel et al., 1999), which can simulate solute transport in variably-saturated porous media, taking into account the effects of salt concentration on water density and water viscosity (Boufadel et al., 1999; Boufadel, 2000). The MARUN code has been verified and validated extensively (Li et al., 2008; Li and Boufadel, 2010; Xia et al., 2010).

The domain for numerical simulations at each transect includes the intertidal zone and part of the area below the bed of tidal river (Fig. 2). The landward boundary of the mangrove transect is vertical and located at M0, where Dirichlet boundary condition was used for the water table in the saturated zone based on interpolations of the observations at M0. The landward boundary of the bald beach transect is 10 m

HESSD
8, 5123–5163, 2011

landward from the high tide line (or B2), where no-flow boundary condition was used for the water table. The horizontal length of the domain is 130 m for the mangrove transect and 270 m for the bald beach transect (Fig. 2). Both domains are assumed to have an impermeable, horizontal bottom at the elevation of −12.5 m. Since most wells do not completely penetrate the mud zone (low-permeability zone), a hypothetical interface between the mud zone and underlain high-permeability zone was used in the numerical simulation. The depths of the interface at the wells are listed in the last column of Tables 1 and 2, and the approximate location of the interface is depicted in Fig. 2. It is also assumed that there is a thin layer of low-permeability sediments on the bed of the tidal river (Fig. 2). This low-permeability layer was identified to be 1.0 m thick from the river bed surface and its permeability is the same as that of the mud zone.

The resolution of the mesh for both transects varies from ∼0.2 m to ∼0.4 m seaward in the x direction, and from ∼0.3 m in the deep portion (depth >5 m) to 0.13 m in the surface portion (depth ≤5 m) in the vertical direction. The mesh of the mangrove transect contains 41412 nodes and 81472 triangular elements, and that of the bald beach transect, 50796 nodes and 99964 triangular elements.

The types of boundary conditions on the beach surface (the upper boundary of the domain) vary with time and are updated at each time step. On the submerged portion of the beach surface, the water pressure was determined by the tidal seawater column above the beach surface. On the boundaries of the unsaturated zone, which include the unsaturated part of the landward boundary and the beach surface above the tidal level, no-flow boundary conditions were used. No-flow boundary conditions were also used along the domain bottom and the vertical right boundary (middle line of the tidal river). The ground water flow under the tidal bed is assumed to be symmetric with respect to the middle line of the tidal river and thus it can be regarded as a no-flow boundary. A hydrostatic pressure distribution in the domain when time is zero was used as the initial condition and then the model results were obtained after running 100 tidal cycles.

HESSD
8, 5123–5163, 2011

6.2 Results of numerical simulations

Trial and error method was used to estimate hydraulic conductivity. The hydraulic conductivity was found to be $1.0 \times 10^{-8}\,m\,s^{-1}$ for the mud zone and $3.0 \times 10^{-4}\,m\,s^{-1}$ for the high-permeability zone and the loose bank zone of the mangrove transect, and $5.0 \times 10^{-8}\,m\,s^{-1}$ for the mud zone and $9.0 \times 10^{-3}\,m\,s^{-1}$ for the high-permeability zone and the loose bank zone at the bald beach transect. Parameters and their values used in simulations are summarized in Table 5.

Figure 4 shows the observed and simulated time series of water table at all wells except B0. The overall quantitative match between the observations and simulations is excellent, implying the rationality of the previous speculation of the existence of the high-permeability zone below the low-permeability mud at both transects.

Figure 7 shows the average Darcy velocity over the 3-day observation period in the mangrove transect. The flow direction in the mud layer is mainly downward and that in the high-permeability zone is mainly seaward, illustrating that both freshwater recharge from inland and seawater from the mud layer discharged to the tidal river through the high-permeability zone. Figure 8 illustrates the transient distributions of Darcy velocity at different times along the mangrove transect. During low tides, groundwater discharged into the tidal river through the high-permeability zone including the river bank near the low tide mark where the velocity was largest (Fig. 8a). During high tides, the high seawater level drove the groundwater to flow landward (Fig. 8b), and blocked the inland freshwater drainage exit near M8. In this case most of the inland freshwater began to discharge directly from the outcrop of the high-permeability zone near M0. All these simulation results are in line with the speculations in previous section, i.e., there is significant freshwater recharge from inland and the low-permeability marsh soil is underlain by a high-permeability zone in this transect.

Figure 9 presents the average Darcy velocity over the observation period in the bald beach transect. The pattern of time-averaged flow is similar to that in the mangrove transect (Fig. 7) except that there was no inland freshwater recharge in the bald beach

HESSD
8, 5123–5163, 2011

transect. Note that the magnitude of the average velocity in the bald beach transect was much larger than that in the mangrove transect due to the difference of the permeability. Fig. 10 depicts the distributions of Darcy velocity at low and high tides along the bald beach transect. During low tides (Fig. 10a), seawater from the outcrop of the high-permeability zone in the high intertidal zone and from the mud layer discharged to the tidal river through the high-permeability zone, which is similar to the case of the mangrove transect (Fig. 8a). During high tides, a small-scale local circulation of seawater-groundwater formed in the high intertidal zone ($-10\,\mathrm{m} \leq x \leq 20\,\mathrm{m}$) at the bald beach transect (Fig. 10b). Despite of this local circulation, the overall flow pattern in this transect is similar to that of the mangrove transect (Fig. 8b). The excellent match between the simulated and observed water tables in the bald beach transect indicated the rationality of the no-flow boundary condition used along the landward boundary of this transect, that is, the inland freshwater recharge is negligible there. These simulation results also verified the presence of a high-permeability zone underlain the less-permeable mud zone.

From a perspective of the submarine groundwater discharge (SGD) or seawater-groundwater circulation, seawater mainly infiltrates the high intertidal zone, groundwater discharges into the tidal creek near the low tide mark (Fig. 11). At mangrove transect, the simulated total outflow flux is $3.94\,\mathrm{m^3\,m^{-1}\,d^{-1}}$. The inland freshwater recharge flux was estimated to be $1.78\,\mathrm{m^3\,m^{-1}\,d^{-1}}$, thus tidal-induced SGD was $2.15\,\mathrm{m^3\,m^{-1}\,d^{-1}}$. At bald beach transect, the estimated tidal-induced SGD was $5.96\,\mathrm{m^3\,m^{-1}\,d^{-1}}$. Note that the seawater-groundwater circulation and SGD at both transects occurred mainly through the high-permeability zone and its outcrops at high and low intertidal zones (Figs. 2, 7, 10 and 11).

HESSD
8, 5123–5163, 2011

7 Discussions

7.1 Similarity of the two transects

Both transects have flat intertidal topography. The mean gradient is 0.0174 for the mangrove transect and 0.014 for the bald beach transect, thus the influence of topography difference on the mangrove growth along the two transects can be excluded. Both transects were subject to the similar tidal action. Similar water table variations were observed in the high, middle and lower intertidal zones of the two transects, respectively. Each transect has a low-permeability zone of mud and underlying high-permeability zone with outcrops at high and low tide lines. On both transects, there were tide-induced seawater-groundwater circulations. The seawater infiltrated the high-permeability zones mainly through its outcrop near the high intertidal zones. The pore water in the high permeability zones discharged to the tidal river near the low tide mark. This intertidal seawater-groundwater circulation is similar to those described by many previous studies (Li and Jiao, 2003; Robinson et al., 2006, 2007a, b, c; Gibbes et al., 2008a, b; Li et al., 2008), and qualitatively has considerable contribution to the total submarine groundwater discharge.

7.2 Ecological implications

Similar phenomena to our mangrove transect were observed in tidal marshes at other places in the world. Harvey et al. (1987) identified that subsurface pore water in Spartina marsh, Chesapeake Bay was mainly discharged from the marsh interior toward the creek bank during exposure of the marsh surface. Yelverton and Hackney (1986) calculated that over 90 % flux of pore water was exported within 2 m of the creek bank to a tidal creek in a marsh of North Carolina. The numerical modeling results conducted by Gardner (2005) showed that the locus of maximum seepage flux from salt marsh sediments occurs at or near the intersection of the creek bank and the channel water surface regardless of the geomorphic configuration. Gardner (2007)

HESSD
8, 5123–5163, 2011

explored the effects of marsh stratigraphy on the seepage of pore water into tidal creeks by employing a two-layer structure: a sand layer (high-permeability zone) underlying the surface mud layer (low-permeability zone). He found that if the mud-sand boundary lies beneath the creek, the seepage dynamics will be the same as those of a purely mud marsh as shown by Gardner (2005), which is in line with our speculated situation shown in Fig. 2. However, if the sand layer is directly connected to the creek bottom, the increased seepage will largely emerge from the creek bottom rather than the creek bank just like the case in a tidal marsh in New England reported by Howes et al. (1996), where groundwater discharge rates conducted by sub-marsh aquifer to the marsh are largest at the creek beds in the absence of mud and at seepage zones near the boundary between the marsh and upland areas.

We observed that the mangrove species in the lower intertidal zone (near M7) were different from those in the middle and high intertidal zones (between M1-M6). Plants in the lower intertidal zone do not have aerial roots (roots that extend upward above the ground surface for respiration), but plants in the middle and high intertidal zone have aerial roots (see Fig. 6). We speculate that this zonation is caused by the root respiration condition determined by the tidal groundwater hydraulics in the marsh. One notes that during low tides the water table dropped ~0.9 m from the ground surface at M7 but stayed almost as high as the ground surface at M1-M6 (Fig. 4). The deep dropping of water table at M7 during low tides allowed filling of air into the soil pores, improved the root respiration condition for plants growing near the tidal river bank. Thus the plants growing near M7 do not need aerial roots. The plants growing between M1 and M6 need aerial roots since their rhizosphere is always saturated, thereby preventing the normal root respiration. In addition, the plant stem density (number of culms per squared meter) was higher near the tidal river bank than in the middle and high intertidal zone, a scenario similar to that reported by Mendelssohn et al. (1981) and Dacey and Howes (1984) that some salt marsh plant species grow better near tidal creeks than in the inner marsh areas. The impacts of root respiration condition on the plant growing status in tidal marshes were discussed by many researchers (Ursino et

HESSD
8, 5123–5163, 2011

al., 2004; Li et al., 2005; Marani et al., 2005, 2006; Wilson and Gardner, 2005, 2009; Tossatto et al., 2009). Li et al. (2005) demonstrated that the optimal plant root aeration condition in a homogeneous tidal marsh transect always occurs near the tidal creek, which may explain the previous observations of Mendelssohn et al. (1981) and Dacey and Howes (1984). Our water table observation along the mangrove transect again indicated that plant root aeration condition is better near the tidal river bank (M7) than in the inner marsh areas (M1-M6), and is influenced not only by the topography, but also by the soil heterogeneity (the hydraulic conductivity of the soil near M7 is several orders of magnitude greater than that in the inner marsh areas between M1 and M6).

8 Conclusions

This paper identified the hydrogeological factors leading to bald beaches among the mangrove marshes in Dongzhaigang National Nature Reserve, China. Based on the field measurements and numerical simulations of water level, the two transects investigated were found to have a mud-sand two-layered structure, which plays a key role in the hydrological regime of study areas. Both the observed water tables at wells in inland and high intertidal zone indicated zero inland freshwater recharge into the bald beach transect. Numerical simulations demonstrated that significant freshwater recharge occurred in the mangrove transect. These results suggest that the bald beach is most probably due to the lack of freshwater recharge for generating brackish and aeration beach soil conditions essential to mangrove growth. The freshwater recharge here may also help limit the buildup of salt in the root zone caused by evapotranspiration, and enhance salt removal which may further increase the production of marsh grasses and influence their spatial distribution.

Owing to the importance of inland groundwater on the mangrove marshes revealed in this paper, preventing the inland groundwater from pollution and relieving the influence of land-oriented contaminants on the mangrove marshes will offer effective protection for coastal mangrove forests. On the other hand, observations from many

HESSD
8, 5123–5163, 2011

spill events around the world have shown that mangroves were severely impacted by oil exposures (Krebs and Burns, 1977; Jackson et al., 1989; Tam et al., 2005), and they are particularly difficult to protect and clean up once a spill has occurred because they are physically intricate and relatively hard to access. In the present study, a loose bank zone was found on both transects, which improves the plant root aeration condition near the tidal river bank. However, this loose bank zone possibly also provides preferential path for spilled oil to enter the marshes and inversely blocked the root soil aeration. All these findings may provide new insights into the management and restoration of these types of coastal ecological systems. There are many mangrove systems in the world that are similar to Dongzhaigang. Such examples include tidal marshes in New England (Howes et al., 1996), in Gazi Bay in Kenya (Kitheka, 1996), in Inhaca Island in Mozambique (Hoguane et al., 1999), and in north Brazil (Schwendenmann et al., 2006). The model described here may apply in these tidal marsh systems.

Acknowledgements. This research is supported by the National Natural Science Foundation of China (NSFC, No. 40672167), NSFC Outstanding Young Scientist Grant (No. 41025009), and the 111 Project (B08030). We are grateful to Mr. Zhiming Han (Hainan Geo-Environment Monitoring Institute) for his help for the fieldwork. The fieldwork was completed with the assistance from the project team members including Shuang Liu, and Xiaolong Geng from Anshan Normal University, Yuchen Zhang, Fangxuan He, and Li Wang from Liaoning Normal University, Shi Chen, Ye Tian, Chao Liu, Qiaona Guo, Guohui Li, Ying Yang, and Pingping Sun from China University of Geosciences (Wuhan).

References

Akamatsu, Y., Ikeda, S., and Toda, Y.: Transport of nutrients and organic matter in a mangrove swamp, Estuarine Coastal and Shelf Science, 82, 233–242, 2009.

Alber, M., Swenson, E. M., Adamowicz, S. C., and Mendelssohn, I. A.: Salt marsh dieback: An overview of recent events in the US, Estuarine Coastal and Shelf Science, 80, 1–11, 2008.

Bosire, J. O., Dahdouh-Guebas, F., Walton, M., Crona, B. I., Lewis, R. R., Field, C., Kairo, J.

HESSD

8, 5123–5163, 2011

G., and Koedam, N.: Functionality of restored mangroves: A review, Aquatic Botany, 89, 251–259, 2008.
Boufadel, M. C., Suidan, M. T., and Venosa, A. D.: A numerical model for density-and-viscosity-dependent flows in two-dimensional variably saturated porous media, J. Contam. Hydrol., 37, 1–20, 1999.
Boufadel, M. C.: A mechanistic study of nonlinear solute transport in a groundwater-surface water system under steady state and transient hydraulic conditions, Water Resour. Res., 36, 2549–2565, 2000.
Chapman, V. J.: Studies in salt marsh ecology: sections i to iii, J. Ecol., 26, 144–179, 1938.
Chapman, V. J.: Studies in salt marsh ecology: sections vi to vii, J. Ecol., 28, 118–152, 1940.
Chapman, V. J.: Wet Coastal Ecosystem, Eslevier Scientific Publishing Company, Amsterdam, 1977.
Clarke, L. D. and Hannon, N. J.: The mangrove swamp and salt marsh communities of the Sydney District: III. Plant growth in relation to salinity and waterlogging, J. Ecol., 58, 351–369, 1970.
Dacey, J. W. H. and Howes, B. L.: Water uptake controls water table movement and sediment oxidation in short spartina marsh, Science, 224, 487–489, 1984.
Dittmar, T., Hertkorn, N., Kattner, G., and Lara, R. J.: Mangroves, a major source of dissolved organic carbon to the oceans, Global Biogeochem. Cy., 20, Gb1012, doi:10.1029/2005GB002570, 2006.
Duke, N. C., Ball, M. C., and Ellison, J. C.: Factors Influencing Biodiversity and Distributional Gradients in Mangroves, Global Ecol. Biogeogr., 7, 27–47, 1998.
Duke, N. C., Meynecke, J. O., Dittmann, S., Ellison, A. M., Anger, K., Berger, U., Cannicci, S., Diele, K., Ewel, K. C., Field, C. D., Koedam, N., Lee, S. Y., Marchand, C., Nordhaus, I., and Dahdouh-Guebas, F.: A world without mangroves, Science, 317, 41–42, 2007.
Field, C. B., Osborn, J. G., Hoffman, L. L., Polsenberg, J. F., Ackerly, D. D., Berry, J. A., Bjorkman, O., Held, A., Matson, P. A., and Mooney, H. A.: Mangrove Biodiversity and Ecosystem Function, Global Ecol. Biogeogr., 7, 3–14, 1998.
Fu, G. A.: The mangroves of Dongzhai Gang Natural Reserve, Hainan, Guihaia, 15, 340–346, 1995 (in Chinese).
Gardner, L. R. and Porter, D. E.: Stratigraphy and geologic history of a southeastern salt marsh basin, North Inlet, South Carolina, USA, Wetl. Ecol. Manag., 9, 371–385, 2001.
Gardner, L. R.: Role of geomorphic and hydraulic parameters in governing pore water seepage

HESSD
8, 5123–5163, 2011

from salt marsh sediments, Water Resour. Res., 41, W07010, doi:10.1029/2004WR003671, 2005.
Gardner, L. R.: Role of stratigraphy in governing pore water seepage from salt marsh sediments, Water Resour. Res., 43, W07502, doi:10.1029/2006WR005338, 2007.
Gardner, L. R.: Comment on "Spatial organization and ecohydrological interactions in oxygen-limited vegetation ecosystems" by Marco Marani et al., Water Resour. Res., 45, W05603, doi:10.1029/2007WR006165, 2009.
Gibbes, B., Robinson, C., Carey, H., Li, L., and Lockington, D.: Tidally driven pore water exchange in offshore intertidal sandbanks: Part I. Field measurements, Estuar. Coast. Shelf S., 79, 121–132, 2008a.
Gibbes, B., Robinson, C., Li, L., Lockington, D., and Li, H. L.: Tidally driven pore water exchange within offshore intertidal sandbanks: Part II numerical simulations, Estuar. Coast. Shelf S., 80, 472–482, 2008b.
Gilman, E. L., Ellison, J., Duke, N. C., and Field, C.: Threats to mangroves from climate change and adaptation options: A review, Aquatic Botany, 89, 237–250, 2008.
Guo, H. P., Jiao, J. J., and Li, H. L.: Groundwater response to tidal fluctuation in a two-zone aquifer, J. Hydrol., 381, 364–371, 2010.
Harvey, J. W., Germann, P. F., and Odum, W. E.: Geomorphological control of subsurface hydrology in the creekbank zone of tidal marshes, Estuar. Coast. Shelf S., 25, 677–691, 1987.
Hemond, H. F. and Fifield, J. L.: Subsurface flow in a salt marsh peat, Limnol. Oceanogr., 27, 126–136, 1982.
Hoguane, A. M., Hill, A. E., Simpson, J. H., and Bowers, D. G.: Diurnal and tidal variation of temperature and salinity in the Ponta Rasa Mangrove swamp, Mozambique, Estuar. Coast. Shelf S., 49, 251–264, 1999.
Howes, B. L., Weiske, P. K., Goehringer, D. D., and Teal., J. M.: Interception of freshwater and nitrogen transport from uplands to coastal waters: the role of saltmarshes, in: Estuarine Shores: Hydrological, Geomorphological and Ecological Interactions, edited by: Nordstrom, K. and Roman, C., Wiley Interscience, Sussex, England, 287–310, 1996.
Hughes, C. E., Binning, P., and Willgoose, G. R.: Characterisation of the hydrology of an estuarine wetland, J. Hydrol., 211, 34–49, 1998.
Jackson, J. B. C., Cubit, J. D., Keller, B. D., Batista, V., Burns, K., Caffey, H. M., Caldwell, R. L., Garrity, S. D., Getter, C. D., Gonzalez, C., Guzman, H. M., Kaufmann, K. W., Knap, A.

HESSD
8, 5123–5163, 2011

H., Levings, S. C., Marshall, M. J., Steger, R., Thompson, R. C., and Weil, E.: Ecological Effects of a Major Oil Spill on Panamanian Coastal Marine Communities, Science, 243, 37–44, 1989.
Kitheka, J. U.: Water circulation and coastal trapping of brackish water in a tropical mangrove-dominated bay in Kenya, Limnol. Oceanogr., 41, 169–176, 1996.
Kjerfve, B.: Manual for investigation of hydrological processes in mangrove ecosystems, UNESCO/UNDP Project, Research and its Application to the Management of the Mangroves of Asia and the Pacific (RAS/86/120), 1990.
Krauss, K. W., Lovelock, C. E., McKee, K. L., Lopez-Hoffman, L., Ewe, S. M. L., and Sousa, W. P.: Environmental drivers in mangrove establishment and early development: A review, Aquatic Botany, 89, 105–127, 2008.
Krebs, C. T. and Burns, K. A.: Long-term effects of an oil spill on populations of the salt-marsh crab uca pugnax, Science, 197, 484–487, 1977.
Kristensen, E., Bouillon, S., Dittmar, T., and Marchand, C.: Organic carbon dynamics in mangrove ecosystems: A review, Aquat. Bot., 89, 201–219, 2008.
Li, H. L. and Jiao, J. J.: Tide-induced seawater-groundwater circulation in a multi-layered coastal leaky aquifer system, J. Hydrol., 274, 211–224, 2003.
Li, H. L., Li, L., and Lockington, D.: Aeration for plant root respiration in a tidal marsh, Water Resour. Res., 41, W06023, doi:10.1029/2004WR003759, 2005.
Li, H. L., Boufadel, M. C., and Weaver, J. W.: Tide-induced seawater-groundwater circulation in shallow beach aquifers, J. Hydrol., 352, 211–224, 2008.
Li, H. L. and Boufadel, M. C.: Long-term persistence of oil from the Exxon Valdez spill in two-layer beaches, Nat. Geosci., 3, 96–99, 2010.
Liu, J. G. and Diamond, J.: China's environment in a globalizing world, Nature, 435, 1179–1186, 2005.
Lugo, A. E. and Snedaker, S. C.: The ecology of mangroves, Annual Review of Ecology, Evolution, and Systematics (formerly, Annual Review of Ecology and Systematics), 5, 39–64, 1974.
Luther, G. W., III, Church, T. M., Scudlark, J. R., and Cosman, M.: Inorganic and organic sulfur cycling in salt-marsh pore waters, Science, 232, 746–749, 1986.
Marani, M., Ursino, N., and Silvestri, S.: Reply to comment by Alicia M. Wilson and Leonard Robert Gardner on "Subsurface flow and vegetation patterns in tidal environments", Water Resour. Res., 41, W07022, doi:10.1029/2004WR003722, 2005.

HESSD
8, 5123–5163, 2011

Marani, M., Silvestri, S., Belluco, E., Ursino, N., Comerlati, A., Tosatto, O., and Putti, M.: Spatial organization and ecohydrological interactions in oxygen-limited vegetation ecosystems, Water Resour. Res., 42, W06D06, doi:10.1029/2005WR004582, 2006.
Mendelssohn, I. A., McKee, K. L., and Patrick, W. H.: Oxygen deficiency in Spartina alterniflora roots: Metabolic adaptation to anoxia, Science, 214, 439–441, 1981.
Merritt, M. L.: Estimating hydraulic properties of the Floridian aquifer sytem by analysis of earth-tide, ocean-tide, and barometric effects, Collier and Hendry Counties, Florida, Tallahassee, Florida, 69, 2004.
Montalto, F. A., Steenhuis, T. S., and Parlange, J. Y.: The hydrology of Piermont Marsh, a reference for tidal marsh restoration in the Hudson river estuary, New York, J. Hydrol., 316, 108–128, 2006.
Nagelkerken, I., Blaber, S. J. M., Bouillon, S., Green, P., Haywood, M., Kirton, L. G., Meynecke, J. O., Pawlik, J., Penrose, H. M., Sasekumar, A., and Somerfield, P. J.: The habitat function of mangroves for terrestrial and marine fauna: A review, Aquat. Bot., 89, 155–185, 2008.
Tide table: http://www.coi.gov.cn, access: Accessed September 2, 2007, 2008.
Nuttle, W. K. and Harvey, J. W.: Fluxes of water and solute in a coastal wetland sediment. I. The contribution of regional groundwater discharge, J. Hydrol., 164, 89–107, 1995.
Pennings, S. C. and Callaway, R. M.: Salt Marsh Plant Zonation: The Relative Importance of Competition and Physical Factors, Ecology, 73, 681–690, 1992.
Robinson, C., Gibbes, B., and Li, L.: Driving mechanisms for groundwater flow and salt transport in a subterranean estuary, Geophys. Res. Lett., 33, L03402, doi:10.1029/2005GL025247, 2006.
Robinson, C., Gibbes, B., Carey, H., and Li, L.: Salt-freshwater dynamics in a subterranean estuary over a spring-neap tidal cycle, J. Geophys. Res.-Oceans, 112, C09007, doi:10.1029/2006JC003888, 2007a.
Robinson, C., Li, L., and Barry, D. A.: Effect of tidal forcing on a subterranean estuary, Adv. Water Resour., 30, 851–865, 2007b.
Robinson, C., Li, L., and Prommer, H.: Tide-induced recirculation across the aquifer-ocean interface, Water Resour. Res., 43, W07428, doi:10.1029/2006WR005679, 2007c.
Schwendenmann, L., Riecke, R., and Lara, R.: Solute dynamics in a North Brazilian mangrove: the influence of sediment permeability and freshwater input, Wetl. Ecol. Manage., 14, 463–475, 2006.
Selvam, V.: Environmental classification of mangrove wetlands of India, Current Science, 84,

HESSD
8, 5123–5163, 2011

757–765, 2003.
Silvestri, S., Defina, A., and Marani, M.: Tidal regime, salinity and salt marsh plant zonation, Estuar. Coast. Shelf S., 62, 119–130, 2005.
Spalding, M., Blasco, F., and Field, C.: World mangrove atlas, International Society for Mangrove Ecosystems, Japan: Okinawa, 178 pp., 1997.
Steudler, P. A. and Peterson, B. J.: Contribution of gaseous sulphur from salt marshes to the global sulphur cycle, Nature, 311, 455–457, 1984.
Tam, N. F. Y., Wong, T. W. Y., and Wong, Y. S.: A case study on fuel oil contamination in a mangrove swamp in Hong Kong, Mar. Pollut. Bull., 51, 1092–1100, 2005.
Tossatto, O., Belluco, E., Silvestri, S., Ursino, N., Comerlati, A., Putti, M., and Marani, M.: Reply to comment by L. R. Gardner on "Spatial organization and ecohydrological interactions in oxygen-limited vegetation ecosystems", Water Resour. Res., 45, W05604, doi:10.1029/2007WR006345, 2009.
Ursino, N., Silvestri, S., and Marani, M.: Subsurface flow and vegetation patterns in tidal environments, Water Resour. Res., 40, W05115, doi:10.1029/2003WR002702, 2004.
Valiela, I. and Teal, J. M.: The nitrogen budget of a salt marsh ecosystem, Nature, 280, 652–656, 1979.
Valiela, I., Bowen, J. L., and York, J. K.: Mangrove forests: One of the world's threatened major tropical environments, Bioscience, 51, 807–815, 2001.
Wilson, A. M. and Gardner, L. R.: Comment on "Subsurface flow and vegetation patterns in tidal environments" by Nadia Ursino, Sonia Silvestri, and Marco Marani, Water Resour. Res., 41, W07021, doi:10.1029/2004WR003554, 2005.
Wilson, A. M. and Gardner, L. R.: Tidally driven groundwater flow and solute exchange in a marsh: Numerical simulations, Water Resour. Res., 42, W01405, doi:10.1029/2005WR004302, 2006.
Wolanski, E. and Ridd, P.: Tidal mixing and trapping in mangrove swamps, Estuar. Coast. Shelf S., 23, 759–771, 1986.
Woodroffe, C. D., Thom, B. G., and Chappell, J.: Development of widespread mangrove swamps in mid-Holocene times in northern Australia, Nature, 317, 711–713, 1985.
Xia, Y. Q., Li, H. L., Boufadel, M. C., and Sharifi, Y.: Hydrodynamic factors affecting the persistence of the Exxon Valdez oil in a shallow bedrock beach, Water Resour. Res., 46, W10528, doi:10.1029/2010WR009179, 2010.
Xin, P., Jin, G., Li, L., and Barry, D. A.: Effects of crab burrows on pore water flows in salt

HESSD
8, 5123–5163, 2011

marshes, Adv. Water Resour., 32, 439–449, 2009.

Ye, Y. and Lu, C.: Dynamics of CH4 in soil under *Aegiceras Corniculatum* mangrove at Changning estuary of Hainan Island, Journal of Tropical Oceanography, 20, 35–42, 2001. (in Chinese)

Yelverton, G. F. and Hackney, C. T.: Flux of dissolved organic carbon and pore water through the substrate of a Spartina alterniflora marsh in North Carolina, Estuar. Coast. Shelf S., 22, 255–267, 1986.

HESSD

8, 5123–5163, 2011

Table 1. Locations and depths of wells at the mangrove transect M-M′.

Locations	Distance (m)	Elevation (m)	Well length above surface (m)	Well length below surface (m)	Thickness of mud layer (m)
M0	0.000	1.615	0.67	1.33	0.8
**M*1	1.038	1.582	/*	/	1.0
M1	7.679	1.367	0.65	1.35	2.5
M2	21.081	1.366	0.68	1.32	2.5
M3	33.291	1.259	0.53	1.47	2.6
M4	47.331	1.133	0.57	1.43	3.0
M5	61.719	1.375	0.52	1.48	3.5
M6	75.985	1.435	0.51	1.49	3.7
M7	90.096	1.284	0.38	1.62	0.4
M8	98.378	0.273	0.49	1.51	0.0
M*2	107.0	−1.5	/	/	1.0
M*3	130.0	−1.5	/	/	1.0

* "/" means not available.
** M*1, M*2, and M*3 are only used to control the geometry of the surface and interfaces, no wells were installed at these locations.

HESSD
8, 5123–5163, 2011

Table 2. Locations and depths of wells at the bald beach transect B-B′.

Locations	Distance (m)	Elevation (m)	Well length above surface (m)	Well length below surface (m)	Thickness of mud layer (m)
B0	−33.000	3.611	0.23	3.77	/
**B_{LB}	−10.000	3.737	/	/	0.0
B1	−5.568	2.839	0.44	3.56	2.0
B2	0.000	2.094	0.19	1.81	0.0
B*1	6.369	1.337	/	/	0.0
B3	17.284	1.166	0.38	1.62	0.9
B*2	26.082	1.127	/	/	2.0
B4	44.078	1.048	0.43	1.57	2.5
B5	65.835	0.907	0.50	1.50	2.5
B6	96.196	0.921	0.47	1.53	2.5
B7	158.884	0.527	0.33	1.67	2.5
B*3	191.263	0.237	/	/	0.0
B*4	210.0	−1.5	/	/	1.0
B*5	260.0	−1.5	/	/	1.0

* "/" means not available.
** B_{LB} denotes the landward boundary location, B*1, B*2, B*3, B*4, and B*5 are only used to control the geometry of the surface and interfaces, no wells were installed at these locations.

HESSD
8, 5123–5163, 2011

Table 3. Fitting results of sea tides.

Mangrove transect				Bald beach transect		
Mea sea level h_{MSL} (m)	Component* i	Amplitude A_i (m)	Phase shift ϕ_i (rad)	Mea sea level h_{MSL} (m)	Amplitude A_i (m)	Phase shift ϕ_i (rad)
1.211	1 (O1)	0.505	0.576	1.181	0.598	0.404
	2 (K1)	0.315	0.564		0.432	0.689
	3 (M2)	0.543	−2.562		0.429	−2.623
	4 (S2)	0.050	−1.738		0.146	−2.712
	5 (N2)	0.179	0.704		0.138	0.232

* Detailed explanations can be found in Table 4 of Merritt (2004).

HESSD
8, 5123–5163, 2011

Table 4. Soil characteristics along bald beach transect B-B′.

Well no.	Sample no.	Description	Depth form surface (cm)
B0	29–42	Topsoil of with recognizable plant material Compacted clay Compacted clay with small rocks Compacted clay Compacted clay Compacted clay with silt	0–23 23–44 44–130 130–294 294–370 370–382
B1	106–108 and 117–125	Fine-coarse sand Compacted clay Sandy loam with gravel Sandy loam with gravel	0–10 10–180 180–280 280–372
B2	1–8	Fine-coarse sand Sandy loam Sandy loam with gravel	0–16 16–24 24–98
B3	16–22	Mud with shell Sandy loam	0–33 33–156
B4	23–28	Mud with shell Mud	0–33 33–158
B5	45–50	Mud with shell Mud	0–3 3–154
B6	51–56	Mud with shell Mud	0–3 3–153
B7	126–131	Mud with shell Mud	0–3 3–167

HESSD
8, 5123–5163, 2011

Table 5. Model parameter values used in the numerical simulations.

Symbol	Definition	Unit		Value
α	Capillary fringe parameter of the van Genuchten (1980) model	m^{-1}	Mangrove	0.5 (mud layer) 10.0 (high-permeability zone)
			Bald beach	3.0 (mud layer) 10.0 (high-permeability zone)
n	Grain size distribution parameter of the van Genuchten (1980) model	–	Mangrove	1.2 (mud layer) 5.0 (high-permeability zone)
			Bald beach	1.5 (mud layer) 5.0 (high-permeability zone)
K	Hydraulic conductivity for saturated freshwater	$m\,s^{-1}$	Mangrove	1.0×10^{-8} (mud layer) 3.0×10^{-4} (high-permeability zone)
			Bald beach	5.0×10^{-8} (mud layer) 9.0×10^{-3} (high-permeability zone)
S_0	Specific storage	m^{-1}		10^{-5}
S_r	Residual soil saturation	–		0.01
ϕ	Porosity	–		0.30
CONVP	The convergence criterion of pressure head in the Picard iterative scheme of MARUN code	m		10^{-5}

HESSD
8, 5123–5163, 2011

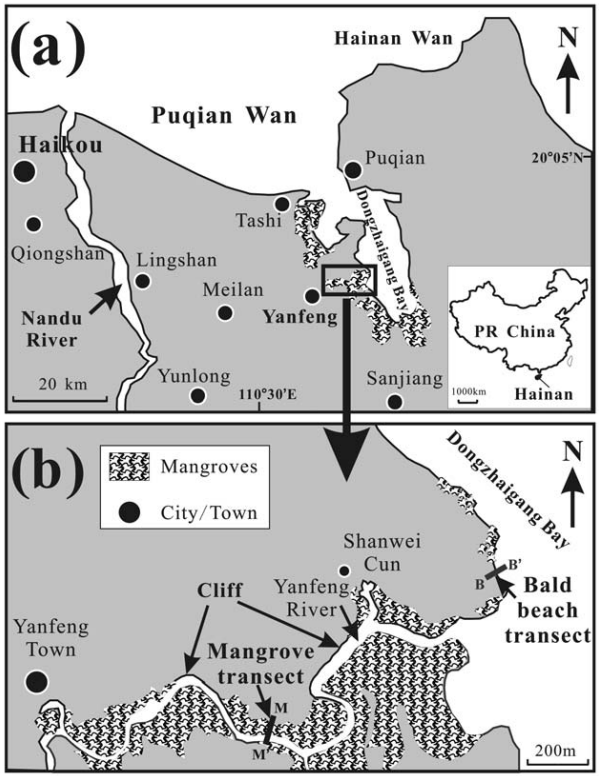

Fig. 1. Location maps of **(a)** Dongzhaigang National Nature Reserve (DNNR), China and **(b)** the mangrove transect M-M′ and the bald beach transect B-B′.

HESSD
8, 5123–5163, 2011

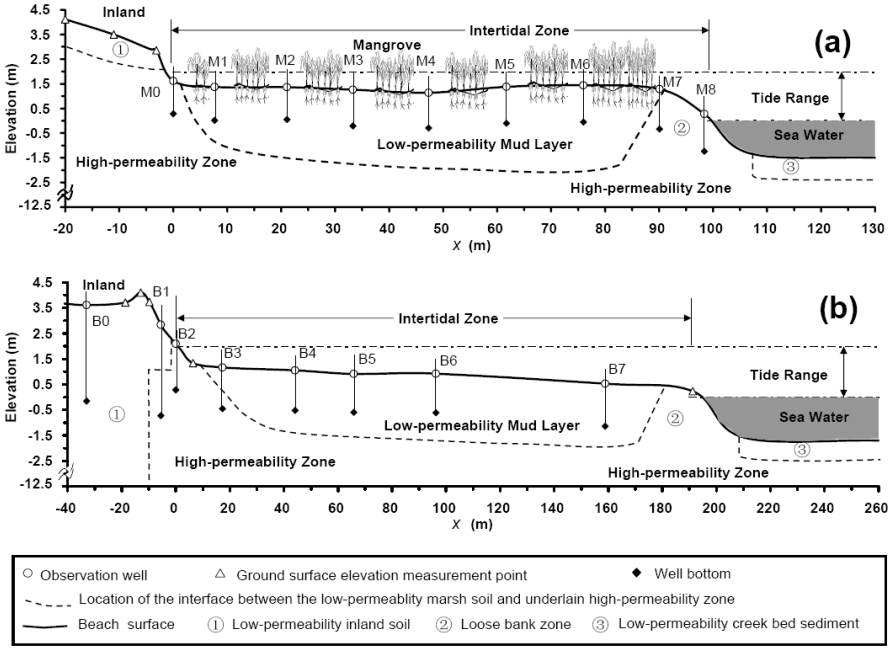

Fig. 2. The cross-section of **(a)** the mangrove transect M-M′ and **(b)** the bald beach transect B-B′. The intertidal zone is located within 0 m ≤ x ≤100 m for the mangrove transect and 0 m ≤ x ≤190 m for the bald beach transect, where x is the seaward distance from the high tide mark. The detailed information about monitoring wells is presented in Fig. 3 and Tables 1 and 2.

HESSD
8, 5123–5163, 2011

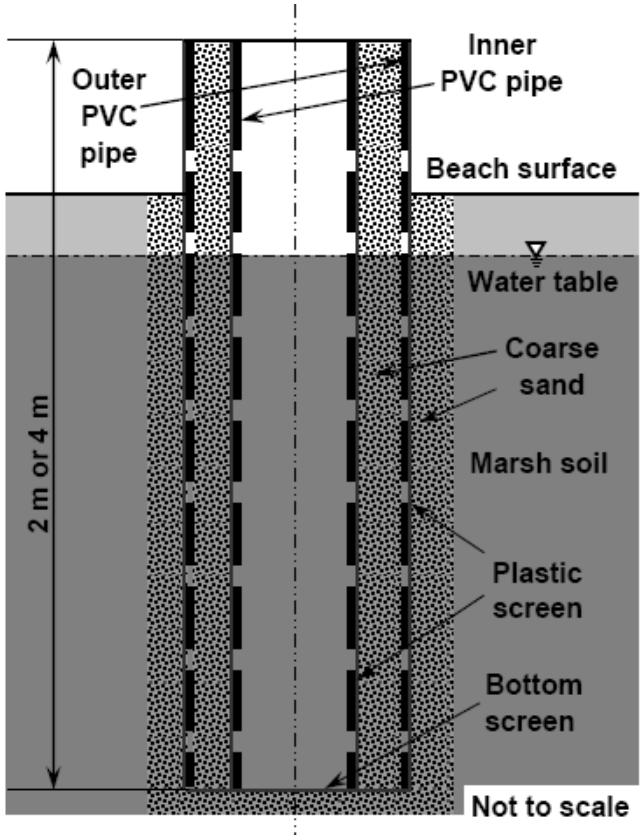

Fig. 3. Installation details of the observation wells.

HESSD
8, 5123–5163, 2011

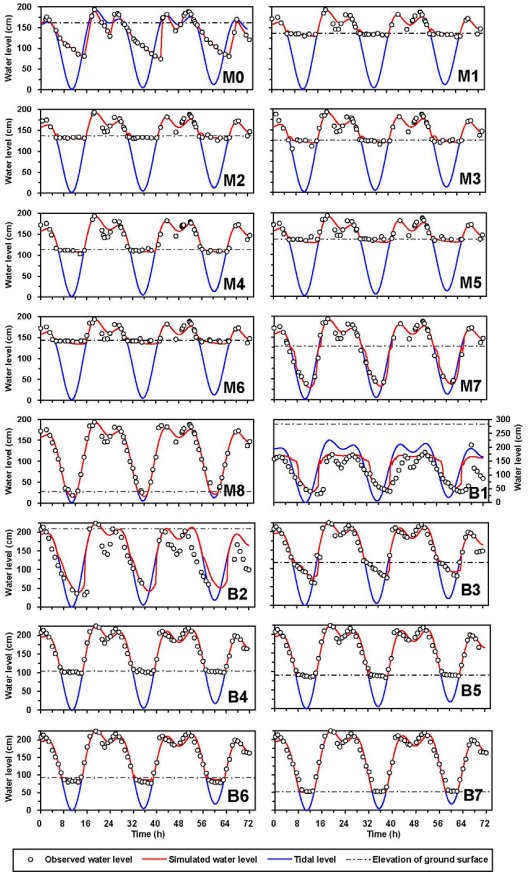

Fig. 4. Simulated (red line) and observed (circles) water levels at wells along two transects. The ground surface elevation (dash dot line) at each well and the tidal level (blue line) are also shown. The initial time of zero hour corresponds to 25 December 2007, 08:00.

HESSD
8, 5123–5163, 2011

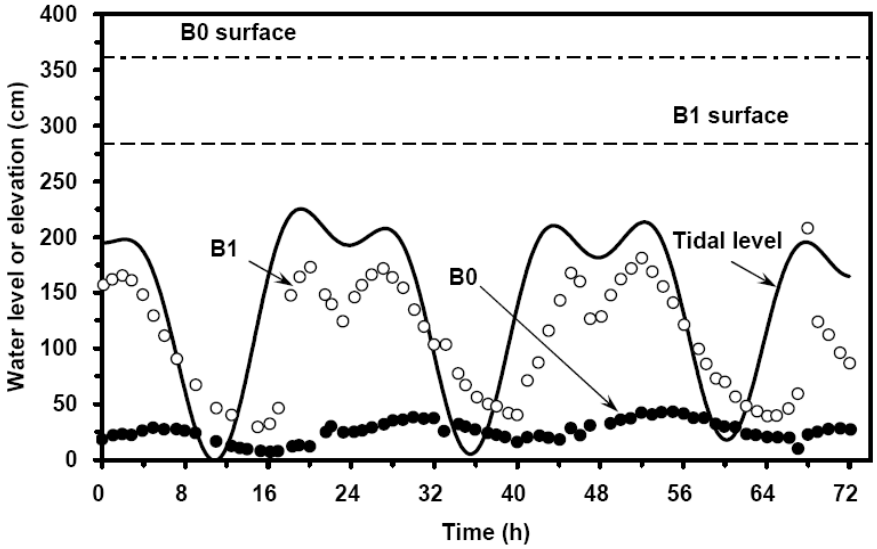

Fig. 5. Comparison of observed water tables at B0 and B1 along the bald beach transect.

HESSD
8, 5123–5163, 2011

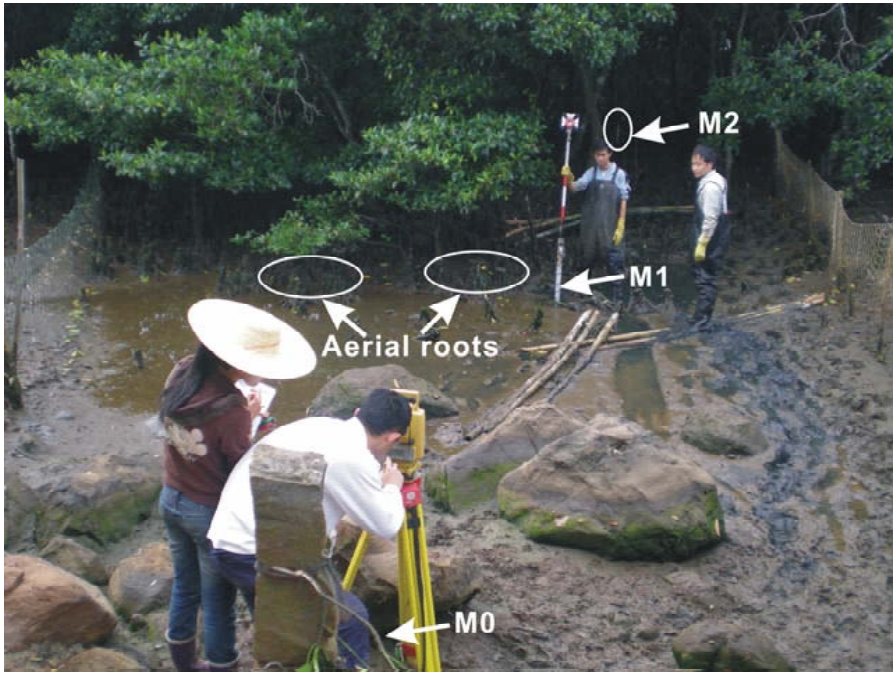

Fig. 6. Boulders (0.2–1.5 m in diameter) exposed near the surface of M0 during low tides. Aerial roots, M1, and M2 are also shown.

HESSD
8, 5123–5163, 2011

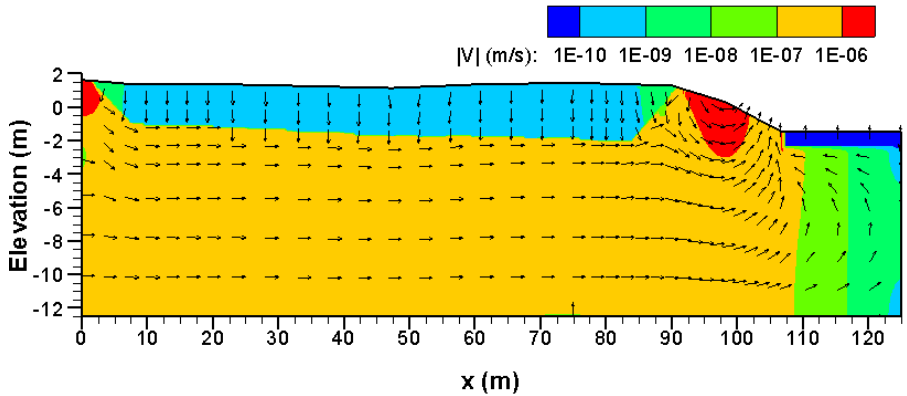

Fig. 7. Average Darcy velocity (banded colorful contours) in the mangrove transect calculated over the observation period of 3 days. Vectors with uniform length were used to indicate the velocity direction only.

HESSD
8, 5123–5163, 2011

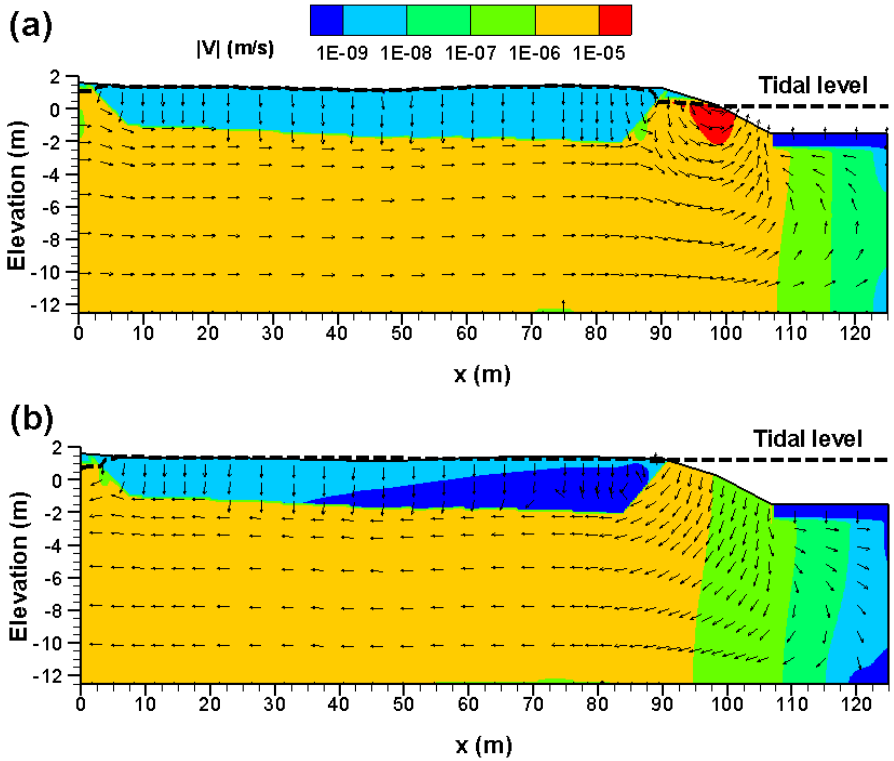

Fig. 8. Darcy velocities (banded colorful contours) in the mangrove transect **(a)** at low tide (Time = 35.5 h) and **(b)** at high tide (Time = 41.0 h). Vectors with uniform length were used to indicate the velocity direction only. The long dash line denotes water table.

HESSD
8, 5123–5163, 2011

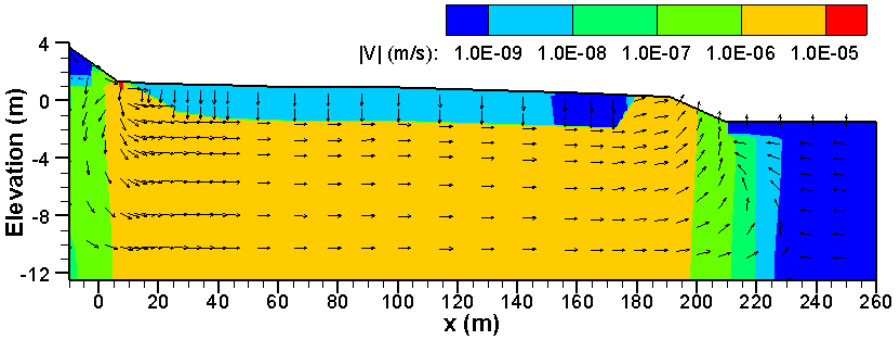

Fig. 9. Average Darcy velocity (banded colorful contours) in the bald beach transect calculated over the observation period of 3 days. Vectors with uniform length were used to indicate the velocity direction only.

HESSD
8, 5123–5163, 2011

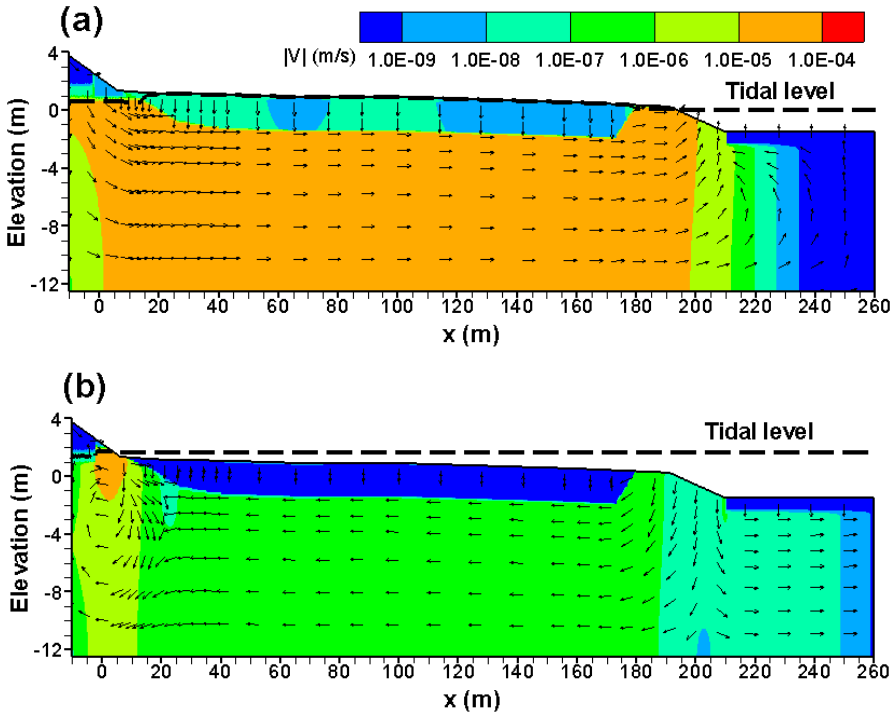

Fig. 10. Darcy velocities (banded colorful contours) in the bald beach transect **(a)** at low tide (Time = 35.5 h) and **(b)** at high tide (Time = 41.0 h). Vectors with uniform length were used to indicate the velocity direction only. The long dashed line denotes water table.

HESSD
8, 5123–5163, 2011

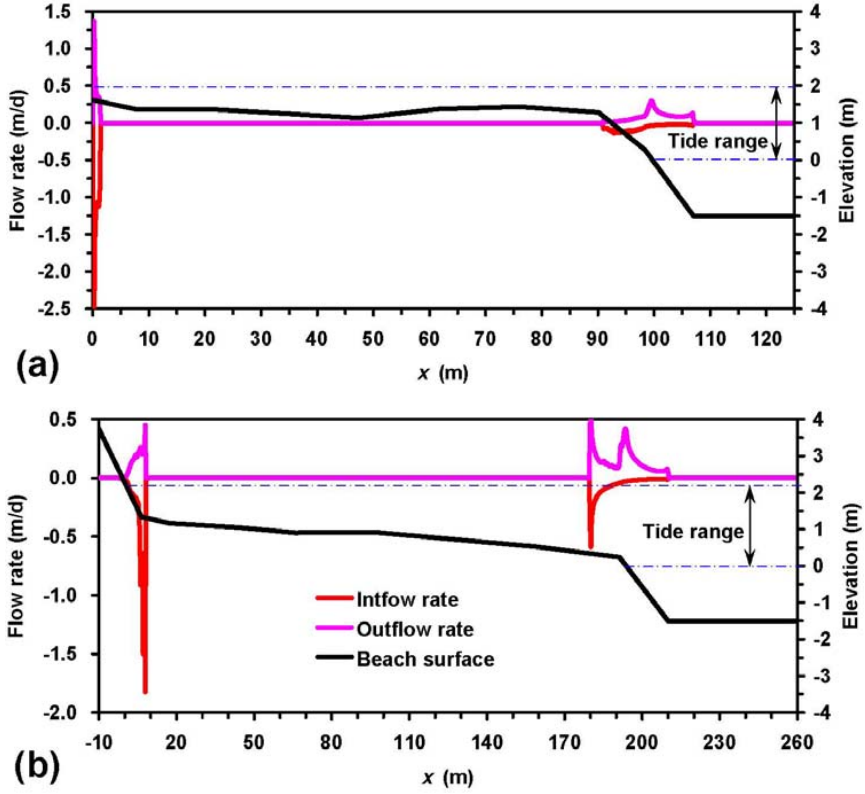

Fig. 11. Average flow rates over the observation period of 3 days along **(a)** the mangrove and **(b)** the bald beach transects. Beach surface and tide range are shown to indicate the distributions of flow rate with them. Note the different scales used for each transect.

HESSD
8, 5123–5163, 2011